

# Interplay of strong correlations and covalency in ionic band insulators

Nagamalleswararao Dasari,<sup>1,\*</sup> Juana Moreno,<sup>2</sup> Mark Jarrell,<sup>2</sup> and N. S. Vidhyadhiraja<sup>1,†</sup>

<sup>1</sup>*Jawaharlal Nehru Centre For Advanced Scientific Research, Jakkur, Bangalore 560064, India.*

<sup>2</sup>*Department of Physics & Astronomy, Louisiana State University, Baton Rouge, LA 70803-4001, USA.*

We have addressed the role of electronic correlations in different kind of band insulators by using two orbital Hubbard model within dynamical mean-field theory (DMFT). We have derived exact results for a single-particle spectral function at Fermi level within DMFT. Our numerical results calculated using impurity solvers namely, hybridization expansion continuous time quantum Monte-Carlo (HY-CTQMC) and multi-orbital iterative perturbation theory (MO-IPT) corroborated with our predicted analytical results.

## I. INTRODUCTION

The recent discovery of interaction-driven topological phases<sup>1-4</sup>, such as, fractional quantum-Hall states, spin-liquids, Kondo-insulators and bosonic topological phases has created a huge interest in, otherwise considered to be mundane, band insulators. Some questions of fundamental interest in band insulators are: how do correlations drive a band insulator into a metal and a Mott insulator(MI) and are correlated band insulators fundamentally different from simple band insulators which have identical charge and spin excitation gaps? Theoretically these issues have been addressed in all dimensions, from one to infinity, by various studies of model Hamiltonians such as the ionic Hubbard model<sup>5-14</sup>, a two-sublattice model with inter-orbital hybridization<sup>15,16</sup>, a two-band Hubbard model with crystal field splitting<sup>17</sup> and a bilayer model with two identical Hubbard planes<sup>18-22</sup>.

The ionic Hubbard model, which comprises a two-sublattice system having orbital energies,  $V$  and  $-V$  with a local Coulomb repulsion, drew a lot of attention after the pioneering work by Arti Garg et. al.,<sup>8</sup>, which showed that correlations can turn a band insulator into a metal and for higher interaction strengths,  $U$ , into a Mott insulator. The  $U - V$  phase diagram, found through a iterated perturbation theory (IPT) solution of the self-consistent impurity problem within dynamical mean field theory (DMFT), exhibited a finite metallic region, which transformed into a line at large  $U$  and  $V$ , as should be the case in the exactly known atomic limit. Later studies using a modified form of IPT, and numerical renormalization group at zero temperature ( $T = 0$ ), and a continuous time quantum Monte-Carlo (CTQMC) study, while confirming the existence of an intervening metallic phase, were not in agreement about the extent of the metallic region. Furthermore, one could ask if there exist parameters other than interaction strength, that could induce metallicity in band insulators, and what would be the interplay of interactions with such an athermal parameter. In this work, we have reconciled the results from the IPT and CTQMC studies, while also answering the latter question within a two orbital Hubbard model with on-site repulsion,  $U$ , between electrons of opposite spin. The novelty of our model is embodied by a parameter “ $x \in [0, 1]$ ” which may be interpreted as the degree of

ionicity, while  $1 - x$  is concomitantly interpreted as the degree of covalency. Such a parametrization permits us to explore the interplay of ionicity and covalency in interacting band insulators. So for  $x = 1$ , we obtain purely ionic band insulators<sup>8</sup> while for  $x = 0$ , the model reduces to purely covalent band insulators<sup>15</sup>. An investigation of correlations in polar-covalent insulators is important in its own right. The characteristic signature of the charge gap in these insulators is an order of few meV and given by inter-orbital hybridization between partially filled bands<sup>15,23</sup>. The canonical example of covalent band insulators are FeSi and FeSb<sub>2</sub><sup>24,25</sup>. The temperature evolution of charge gap in these systems closes at low temperature relative to gap size and the spectral weight in the optical conductivity transfer to high-frequencies ( $\approx 1$  eV) above the gap edge. These two features strongly determine the role of electronic correlations in the covalent band insulators.

The interaction driven metallic region found in Ref<sup>8</sup> for the purely ionic Hubbard model is shown analytically to be just a line of measure zero in the  $U - V$  plane. One of the main findings is that, while the two extremes of  $x = 0$  and  $x = 1$  are indeed band insulators, albeit of different kinds, the  $x = 0.5$  turns out to be a metal even in the non-interacting case. Further, the metal at  $U = 0$  turns into a correlated band insulator even for infinitesimal interactions, and a re-entrant metallic phase is found at higher interactions, beyond which a Mott insulator is obtained. We find a rich phase diagram in the  $U - T$  plane that is strongly dependent on the degree of covalency (or ionicity).

This chapter is organized as follows: In Sec. II, we define the model and methods chosen to study correlation effects in different kinds of band insulators. In Sec. III, first we discuss the analytical results at zero and finite temperatures and then we present and discuss our numerical results. Finally, in Sec. IV, we present our conclusions.

## II. MODELS AND METHODS

We have considered a two orbital Hubbard model with a local Coulomb interaction between two electrons of opposite spin on same orbital. In the second quantized

notation, the Hamiltonian reads,

$$\mathcal{H} = -\mu \sum_{i\alpha\sigma} \hat{n}_{i\alpha\sigma} + \sum_{ij\alpha\beta\sigma} t_{ij}^{\alpha\beta} (c_{i\alpha\sigma}^\dagger c_{j\beta\sigma} + h.c.) + \sum_{i\alpha\sigma} \frac{U}{2} \hat{n}_{i\alpha\sigma} \hat{n}_{i\alpha\bar{\sigma}} \quad (1)$$

$$= \sum_{k\sigma} \begin{pmatrix} c_{kA\sigma}^\dagger & c_{kB\sigma}^\dagger \end{pmatrix} \mathbf{H}_\sigma(\mathbf{k}) \begin{pmatrix} c_{kA\sigma} \\ c_{kB\sigma} \end{pmatrix} + \sum_{i\alpha\sigma} \frac{U}{2} \hat{n}_{i\alpha\sigma} \hat{n}_{i\alpha\bar{\sigma}} \quad (2)$$

where  $c_{i\alpha\sigma}^\dagger (c_{i\alpha\sigma})$  creates (annihilates) an electron at lattice site  $i$ , in orbital  $\alpha = A/B$  with  $S_z$  eigenvalue  $\sigma$ . We set the chemical potential  $\mu = \frac{U}{2}$  so that each unit cell has a total average occupancy of 2 (i.e. half filling). The unit cell thus consists of two orbitals A and B. An equivalent interpretation is the consideration of sublattices A, B. The latter is usually chosen for the ionic Hubbard model. In the equation (2),  $\mathbf{H}_\sigma(\mathbf{k})$  comprises orbital energies, intra-unit-cell hybridization and nearest neighbour inter-unit-cell hopping, namely

$$\mathbf{H}_\sigma(\mathbf{k}) = \mathbf{H}^\sigma(\mathbf{k})_{intra} + \mathbf{H}^\sigma(\mathbf{k})_{inter}.$$

We are mainly interested in local single particle electron dynamics, which is given by the momentum sum of the lattice Green's function,

$$\mathbf{G}_\sigma(\omega^+) = \sum_{\mathbf{k}} [(\omega^+ + \mu)\mathbb{I} - \mathbf{H}_\sigma(\mathbf{k}) - \Sigma_\sigma(\mathbf{k}, \omega^+)]^{-1}, \quad (3)$$

where  $\omega^+ = \omega + i\eta$  and  $\eta \rightarrow 0^+$ , and  $\mathbb{I}$  is the identity matrix. We have calculated the local single particle propagators within the DMFT framework, wherein the single particle irreducible self-energy  $\Sigma_\sigma(\omega^+)$  is local, and will be determined by solving the auxiliary Anderson impurity model. The local, interacting Green's function (equation (3)) may be related to the non-interacting Green's function  $\mathbf{G}_{0\sigma}(\omega^+)$  through the Dyson equation:

$$\mathbf{G}_{0\sigma}^{-1}(\omega^+) = \mathbf{G}_\sigma^{-1}(\omega^+) + \Sigma_\sigma(\omega^+). \quad (4)$$

We construct a non-interacting Hamiltonian  $\mathbf{H}_\sigma(\mathbf{k})$  as an interpolation between an ionic band insulator (IBI) and a covalent insulator (CI) as follows:

$$\mathbf{H}_\sigma(\mathbf{k}, x) = \mathbf{H}_{IBI} + \mathbf{H}_{CI} = x \begin{pmatrix} \Delta & \epsilon_{k\sigma} \\ \epsilon_{k\sigma} & -\Delta \end{pmatrix} + (1-x) \begin{pmatrix} \tilde{\epsilon}_{k\sigma} & V \\ V & -\tilde{\epsilon}_{k\sigma} \end{pmatrix}, \quad (5)$$

where the IBI corresponds to  $x = 1$ , while the CI is obtained at  $x = 0$ , hence  $x$  represents the fraction of ionicity, while  $1 - x$  represents covalency. In the IBI, a two sublattice system has staggered ionic potentials  $\Delta$  and  $-\Delta$  and a  $k$ -dependent hybridization ( $\epsilon_{k\sigma}$ ) between sites on sublattice 1 and 2. The CI is character-

ized by two semicircular bands having opposite sign of the hopping parameter and a  $k$ -independent hybridization  $V$ . The diagonal dispersion in the CI corresponds to intra-band electron hopping, while the off-diagonal dispersion in the IBI corresponds to inter-band electron hopping. By varying the parameter  $x$  from 1 to 0, we can interpolate smoothly between a purely ionic limit (for  $x = 1$ ) and a purely covalent limit ( $x = 0$ ). In other words, the percentage of covalency in the ionic band insulator increases as we decrease  $x$  from 1 to 0.

The motivation to build and study the above Hamiltonian is twofold: (a) There are three primary chemical bonds namely ionic, covalent and metallic bonds. But in practice, a perfect ionic bond does not exist, i.e., any bond has a partial covalency. Quantifying the covalency or the ionicity of a given bond is not without ambiguities<sup>26,27</sup>. Depending upon the percentage of covalency in the ionic bond, properties of the system changes drastically<sup>26,27</sup>. Equation (5) is one the simplest and of course, non-unique, ways of parametrizing a system wherein the bonding has an ionic as well as covalent character. (b) Another perspective from the view point of real materials is that the non-interacting Hamiltonian  $\mathbf{H}_\sigma(\mathbf{k})$  could have both inter-unit cell and intra-unit cell hybridizations, where inter-unit cell hopping is often neglected in model calculations<sup>28</sup>.

Throughout the paper, we have considered the case where  $V = \Delta$  and  $\epsilon_k = \tilde{\epsilon}_k$ . Although these are specific parameter choices, the results we obtain are quite general and applicable to more general choices. The structure of  $\mathbf{H}_\sigma(\mathbf{k}, x)$  determines the form of the impurity Greens functions, which for orbital (or sublattice) 1 is given by,

$$G_{1\sigma}(\omega^+) = \int d\epsilon \frac{\zeta_{2\sigma}(\omega^+, \epsilon) \rho_0(\epsilon)}{\zeta_{1\sigma}(\omega^+, \epsilon) \zeta_{2\sigma}(\omega^+, \epsilon) - [V(1-x) + \epsilon x]^2}, \quad (6)$$

where

$$\zeta_{1\sigma}(\omega^+, \epsilon) = \omega + i\eta + \mu - [Vx + \epsilon(1-x)] - \Sigma_{1\sigma}(\omega^+),$$

$$\zeta_{2\sigma}(\omega^+, \epsilon) = \omega + i\eta + \mu + [Vx + \epsilon(1-x)] - \Sigma_{2\sigma}(\omega^+),$$

and  $\rho_0(\epsilon) = \frac{2}{\pi D} \sqrt{1 - (\epsilon/D)^2}$ .  $D = 1$  is our energy unit and  $\eta \rightarrow 0^+$  is the convergence factor. In the half-filling case, the Hamiltonian has mirror type symmetry between orbitals, which reflects in the impurity Green's function and self-energy in the following way,

$$G_{1\sigma}(\omega^+) = -[G_{2\sigma}(-\omega^+)]^*, \quad (7)$$

$$\Sigma_{1\sigma}(\omega^+) = U - [\Sigma_{2\sigma}(-\omega^+)]^*. \quad (8)$$

By using above self-energy symmetry relation, we can readily show that,

$$\zeta_{1\sigma}(\omega^+, \epsilon) = -[\zeta_{2\sigma}(-\omega^+, \epsilon)]^*, \quad (9)$$

then equation (6) can be written as,

$$G_{1\sigma}(\omega^+) = \int d\epsilon \frac{\zeta_{1\sigma}^*(-\omega^+, \epsilon) \rho_0(\epsilon)}{\zeta_{1\sigma}(\omega^+, \epsilon) \zeta_{1\sigma}^*(-\omega^+, \epsilon) - [V(1-x) + \epsilon x]^2}. \quad (10)$$

Now we are going to present a few analytical results for the density of states (DOS) at the Fermi level ( $\omega = 0$ ) and subsequently, we will discuss our numerical results.

### III. RESULTS AND DISCUSSION

One of the most interesting findings in the case of the ionic Hubbard model was that correlations can turn a band insulator into a metal. In general, the distinction between a metal and insulator for clean systems, can be made based on the low energy single-particle density of states. So, in the following sub-section, we will analyse the conditions for which the  $\omega \rightarrow 0$  DOS is finite.

#### A. Analytical results: $T = 0$

In Ref.<sup>8</sup>, it was assumed that adiabatic continuity to a corresponding non-interacting limit is maintained in the correlated band insulator, as well as in the metallic phase, until of course, a quantum phase transition to the Mott insulator occurs. Following the same, we have found the conditions for metallicity or insulating behaviour, provided a Fermi-liquid expansion of self-energy holds, namely that  $\Sigma(\omega) \xrightarrow{\omega \rightarrow 0} \Sigma(0) + \omega(1-1/Z) + \mathcal{O}(\omega^2)$ . Then, the value of imaginary part of self-energy at zero frequency is  $\text{Im}\Sigma_{1\sigma}(0) = 0$ , and the corresponding density of states (DOS)  $D_{1\sigma}(0) = -\frac{1}{\pi} \text{Im}G_{1\sigma}(0)$  is given by,

$$D_{1\sigma}(0) = \int \frac{d\epsilon \rho_0(\epsilon) \frac{\eta}{\pi}}{\eta^2 + [\text{Re}(\zeta_{1\sigma}(0, \epsilon))]^2 + [V(1-x) + \epsilon x]^2}, \quad (11)$$

where  $\eta \rightarrow 0^+$  and  $\text{Re}(\zeta_{1\sigma}(0, \epsilon)) = [\mu - (Vx + \epsilon(1-x)) - \text{Re}\Sigma_{1\sigma}(0)]$ . For a metallic system there should be a finite DOS at the Fermi level, while in the case of insulators, it should be zero. In the following sub-sections for different values of  $x$ , we are going to find the conditions for existence of metallicity.

#### 1. Ionic band insulator ( $x = 1$ )

By substituting  $x = 1$  in equation (5), the non-interacting  $\mathbf{H}_\sigma(\mathbf{k}, x)$  reduces to:

$$\mathbf{H}_\sigma(\mathbf{K}) = \begin{pmatrix} V & \epsilon_k \\ \epsilon_k & -V \end{pmatrix}. \quad (12)$$

In literature this is often called an ‘‘ionic Hubbard model (IHM)’’, where there are two broad electronic bands with

staggered ionic potentials  $V$  and  $-V$  and  $\epsilon_{k\sigma}$  is the dispersion of the bands. The name ionic band insulator suggests that the non-interacting excitation spectrum ( $E_k = \sqrt{\epsilon_k^2 + V^2}$ ) has a gap due to ionic potential ( $V$ ). The DOS at the Fermi level is given by,

$$D_{1\sigma}(0) = \int \frac{d\epsilon \rho_0(\epsilon) \frac{\eta}{\pi}}{[\eta^2 + \epsilon^2 + (\mu - \text{Re}\Sigma_{1\sigma}(0) - V)^2]}. \quad (13)$$

By taking the limit  $\eta \rightarrow 0^+$ , we get

$$D_{1\sigma}(0) = \int d\epsilon \rho_0(\epsilon) \delta\left(\sqrt{\epsilon^2 + (\mu - \text{Re}\Sigma_{1\sigma}(0) - V)^2}\right). \quad (14)$$

This expression states that if  $\mu - \text{Re}\Sigma_{1\sigma}(0) - V = 0$  then  $D_{1\sigma}(0) = \rho_0(0)$ , else  $D_{1\sigma}(0) = 0$ . For a fixed  $\mu = U/2$  and  $V$ , such a condition is never satisfied in the non-interacting case ( $U = 0$ ), while in the interacting case, since the real part of the self-energy may be expected to be a monotonically varying function of  $U$ , the condition can only be satisfied for a specific  $U$  corresponding to a given  $V$ . Thus, the metallic phase (where  $D_{1\sigma}(0) \neq 0$ ) for the purely ionic band insulator ( $x = 1$ ) exists only on a single line, rather than a finite region in the  $V-U$  phase diagram. Our numerical results validate this inference, as shown later.

#### 2. Covalent band insulator ( $x = 0$ )

In this limit,  $\mathbf{H}_\sigma(\mathbf{k}, x)$  can be written as,

$$\mathbf{H}_\sigma(\mathbf{k}) = \begin{pmatrix} \epsilon_k & V \\ V & -\epsilon_k \end{pmatrix}. \quad (15)$$

Systems defined by the above type of Hamiltonian have been termed ‘‘Covalent band insulators’’ (CBI), where two electronic bands with dispersion  $\epsilon_{k\sigma}$ ,  $-\epsilon_{k\sigma}$  hybridize through a  $\mathbf{k}$ -independent hybridization ( $V$ ). The non-interacting excitation spectrum ( $E_k = \sqrt{\epsilon_k^2 + V^2}$ ) is gapped due to the inter-orbital hybridization  $V$  (which represents covalency). The opposite sign of the dispersion of the two bands ensures a finite gap in non-interacting excitation spectrum,  $E_k$ , for any value of  $V$ . The DOS at the Fermi level, for  $x = 0$ , reduces to the following form (following arguments similar to those for the ionic band insulator),

$$D_{1\sigma}(0) = \int \frac{d\epsilon \rho_0(\epsilon) \frac{\eta}{\pi}}{[\eta^2 + V^2 + (\mu - \text{Re}\Sigma_{1\sigma}(0) - \epsilon)^2]}. \quad (16)$$

By taking the limit  $\eta \rightarrow 0^+$ , we get

$$\begin{aligned} D_{1\sigma}(0) &= \int d\epsilon \rho_0(\epsilon) \delta\left(\sqrt{V^2 + (\mu - \text{Re}\Sigma_{1\sigma}(0) - \epsilon)^2}\right) \\ &= 0 \quad \text{for any } V \neq 0, \end{aligned} \quad (17)$$

since the argument of the Dirac delta function is positive definite. Thus for covalent band insulators, interactions can not close the gap at  $T = 0$ , no matter how strong they are, implying a complete absence of metallicity.

### 3. $x = 0.5$

The mixing parameter  $x = 0.5$  corresponds to the case where the ionicity and covalency are present in an equal proportion and the structure of  $\mathbf{H}_\sigma(\mathbf{k}, x)$  is given by,

$$\mathbf{H}_\sigma(\mathbf{k}) = \frac{1}{2} \begin{pmatrix} V + \epsilon_{k\sigma} & V + \epsilon_{k\sigma} \\ V + \epsilon_{k\sigma} & -(V + \epsilon_{k\sigma}) \end{pmatrix}. \quad (18)$$

The DOS at the Fermi level is given by,

$$D_{1\sigma}(0) = \int \frac{d\epsilon \rho_0(\epsilon) \frac{\eta}{\pi}}{\eta^2 + \frac{(\epsilon+V)^2}{4} + [\mu - \text{Re}\Sigma_{1\sigma}(0) - \frac{(\epsilon+V)}{2}]^2}. \quad (19)$$

In the non-interacting case i.e.,  $U = 0$  ( $\Rightarrow \mu = 0$  and  $\text{Re}\Sigma_{1\sigma}(0)=0$ ),

$$D_{1\sigma}(0) = \int \frac{d\epsilon \rho_0(\epsilon) \frac{\eta}{\pi}}{\eta^2 + \frac{(\epsilon+V)^2}{2}}, \quad (20)$$

$$\begin{aligned} D_{1\sigma}(0) &= \int d\epsilon \rho_0(\epsilon) \delta\left(\frac{\epsilon+V}{\sqrt{2}}\right) = \rho_0(-V) \sqrt{2}, \\ &= \frac{2\sqrt{2}}{\pi D} \sqrt{1 - \left(\frac{-V}{D}\right)^2}. \end{aligned} \quad (21)$$

Thus, the DOS at the Fermi-level is finite even in the non-interacting case, i.e., the ground state is a metal. This can also be proven from the non-interacting excitation spectrum ( $E_k = \sqrt{2}(\epsilon_k + V)$ ), which is gapless. In order to understand if the non-interacting metallic state survives at a finite  $U$ , we go back to equation (19). The DOS at Fermi-level is given by,

$$D_{1\sigma}(0) = \int d\epsilon \rho_0(\epsilon) \times \delta\left(\sqrt{\frac{(\epsilon+V)^2}{4} + \left(\mu - \text{Re}\Sigma_{1\sigma}(0) - \frac{(\epsilon+V)}{2}\right)^2}\right), \quad (22)$$

which is finite only if  $|V| < D$  and  $\frac{U}{2} - \text{Re}\Sigma_{1\sigma}(0) = 0$ . Consider a weakly interacting system, where  $U \rightarrow 0^+$ . Then,  $\frac{U}{2} - \text{Re}\Sigma_{1\sigma}(0) \neq 0$  since  $\text{Re}\Sigma_{1,\sigma}(0) \approx U n_{1\sigma} \neq \frac{U}{2}$ . Thus, the metallic phase exists only at  $U = 0$ , and the system instantly becomes gapped for even an infinitesimal  $U$ . Thus apart from the non-interacting case, we again get a band insulator, albeit correlated, for a range of  $U$  values. With increasing  $U$ ,  $\frac{U}{2} - \text{Re}\Sigma_{1\sigma}(0)$  decreases, since  $n_{1,\sigma} \rightarrow 0.5$ . Thus, a second metallic phase, which is correlated, must arise at a finite  $U$  value when

$\mu - \text{Re}\Sigma_{1\sigma}(0) = 0$ . Thus, an interaction induced band insulator sandwiched between two metallic phases emerges due to local electronic correlations.

### 4. General case: $0.5 < x < 1.0$ and $0 < x < 0.5$

In the general case, the DOS at Fermi level is given by,

$$D_{1\sigma}(0) = \int d\epsilon \rho_0(\epsilon) \delta(g(\epsilon)), \quad (23)$$

where

$$g(\epsilon) = \sqrt{(V(1-x) + \epsilon x)^2 + (\text{Re}(\zeta_{1\sigma}(0, \epsilon)))^2} \quad (24)$$

and  $\text{Re}(\zeta_{1\sigma}(0, \epsilon)) = \mu - \text{Re}\Sigma_{1\sigma}(0) - (Vx + \epsilon(1-x))$ . The DOS at the Fermi level is finite only if  $g(\epsilon) = 0$ , which in turn requires

$$\epsilon = -V \frac{1-x}{x} \quad (25)$$

$$\text{and } \mu - \text{Re}\Sigma_{1\sigma}(0) - 2V \left(1 - \frac{1}{2x}\right) = 0. \quad (26)$$

If equation (26) can be satisfied for some  $U$ , then the DOS will be given by

$$D_{1\sigma}(0) = \frac{1}{\sqrt{x^2 + (1-x)^2}} \frac{2}{\pi D} \sqrt{1 - \left(\frac{V(1-x)}{Dx}\right)^2} \quad (27)$$

For a given  $x$ , whether equation (26) is satisfied or not is completely decided by  $n_{1\sigma}$ . For  $x > 0.5$ , if  $n_{1\sigma} < 0.5$ , then  $\text{Re}\Sigma(0) \approx U n_{1\sigma} < U/2$ , and hence,  $U/2 - \text{Re}\Sigma_{1\sigma}(0) > 0$  i.e. a specific  $U$  might exist which satisfies the condition. If however,  $n_{1\sigma} > 0.5$  then for any  $U$  value the condition is never met. For  $x < 1/2$ , the condition  $\mu - \text{Re}\Sigma(0) = -(1-2x)/x$  is never satisfied unless  $n_{1\sigma} > 0.5$ .

## B. Analytical results: $T > 0$

At low enough temperatures, the expression for Fermi-liquid form of self energy is,  $\text{Im}\Sigma_{1\sigma}(\omega) \propto -\max(\omega^2 + T^2)$ . Thus, equation (10) becomes

$$G_{1\sigma}(0) = \int d\epsilon \rho_0(\epsilon) \times \frac{[i\text{Im}\Sigma_{1\sigma}(0) + \text{Re}(\zeta_{1\sigma}^*(0, \epsilon))]}{[\text{Im}\Sigma_{1\sigma}(0)]^2 + [V(1-x) + \epsilon x]^2 + [\text{Re}(\zeta_{1\sigma}^*(0, \epsilon))]^2}, \quad (28)$$

and the corresponding DOS is

$$D_{1\sigma}(0) = \int d\epsilon \rho_0(\epsilon) \times \frac{-\text{Im}\Sigma_{1\sigma}(0)/\pi}{[\text{Im}\Sigma_{1\sigma}(0)]^2 + [V(1-x) + \epsilon x]^2 + [\text{Re}(\zeta_{1\sigma}^*(0, \epsilon))]^2}. \quad (29)$$

Thus, the Dirac delta functions at  $T = 0$  acquire a finite width due to thermal broadening. However, these resonances are sharply peaked if  $T \rightarrow 0$ . Although the above integral is always finite, a significant density of states is obtained only when  $[V(1-x) + \epsilon x]^2 + [\text{Re}(\zeta_{1\sigma}^*(0, \epsilon))]^2 \leq [\text{Im}\Sigma_{1\sigma}(0)]^2$  which would, in general, be satisfied for a range of  $U$  values. The integral has a maximum value only when  $[V(1-x) + \epsilon x]^2 + [\text{Re}(\zeta_{1\sigma}^*(0, \epsilon))]^2 = 0$ . Thus, at finite temperatures, the single metallic line of  $T = 0$  broadens into a metallic region. This is also corroborated by recent CTQMC calculations<sup>13</sup> for the ionic Hubbard model ( $x = 1$ ), and as shown in the next section, by our results as well.

### C. Numerical results

Now we are going to describe results obtained by the numerical solution of the auxiliary Anderson impurity model of equation (2) within DMFT. As an impurity solver, we have used iterated perturbation theory (IPT)<sup>29</sup> and hybridization expansion continuous-time quantum Monte-Carlo (HY-CTQMC)<sup>30,31</sup> methods at zero temperature and finite temperature respectively. In the numerical calculations, we have fixed  $V = 0.5$ .

#### 1. $x=1$ (ionic band insulator)

At the Hartree level, the self-energy is given by  $\Sigma_{1\sigma} = U n_{1\bar{\sigma}}$ , and hence the excitation spectrum  $\left[ E_k = \sqrt{\epsilon_k^2 + (V - U \frac{\delta n}{2})^2} \right]$  has a gap of  $2\bar{V} = 2(V - U \frac{\delta n}{2})$  where  $\delta n = n_{1\sigma} - n_{2\sigma}$ . So for a given  $\delta n$ , the value of  $\text{Re}\zeta_{1\sigma}(0)$  (i.e.,  $\mu - \text{Re}\Sigma_{1\sigma}(0) - V$ ) is constant with respect to  $U$  and it goes to zero only when  $\delta n = 0$ . Thus, the metallic phase exists in HF-theory only when  $V = 0$  ( $\Rightarrow \delta n = 0$ ) and indeed we observed the same as shown in figure 1(a).

Incorporating dynamics beyond the static (HF) theory leads to a completely different picture. The lower panel of figure 1 shows IPT results for  $\text{Re}\zeta_{1\sigma}(0)$  as a function of  $U$  for  $\delta n = 0.0025$ . With increasing  $U$ ,  $\text{Re}\zeta_{1\sigma}(0)$  starts decreasing and vanishes at a critical value,  $U_c$ . Above this critical interaction strength,  $\text{Re}\zeta_{1\sigma}(0)$  changes its sign. As argued in section III A 1, the vanishing of  $\text{Re}\zeta_{1\sigma}(0)$  signals metallicity, and the result in the lower panel of figure 1 (zoomed in the inset) shows that the metal arises at precisely one value of the interaction strength for a given  $V$  and a fixed  $\delta n$ . The only effect of interactions at the chemical potential ( $\omega = 0$ ) is to induce a static real shift in the orbital energy, which is solely responsible for turning the ionic band insulator into a metal. However, it is important to note that a pure Hartree shift is not sufficient, and dynamics beyond the Hartree level is necessary to obtain the metal. The same qualitative picture holds for other values of the ionic potential ( $V$ ), and hence in the  $U - V$  phase diagram of IHM, the metallic phase

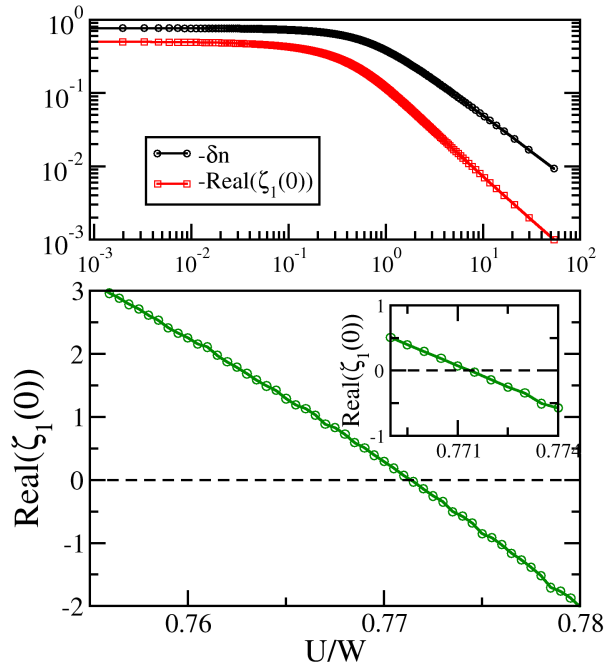


FIG. 1. (color online) Top panel:  $-\delta n = n_{2\sigma} - n_{1\sigma}$  (black circles) and  $-\text{Re}\zeta_{1\sigma}(0)$  (red squares) as a function of  $U$  ( $V = 0.5$ ) obtained within the self-consistent Hartree approximation. The result shows that the system does not metallize for any interaction strength. Lower panel: Zero temperature IPT results for  $\text{Re}\zeta_{1\sigma}(0)$  as a function of  $U$  ( $V = 0.5$ ) for a fixed  $\delta n = 0.0025$ . In the inset, the zero crossing has been zoomed to show that only a single zero crossing is obtained as a function of  $U$  (with  $\eta = 10^{-9}$  and energy unit  $D = \frac{W}{2} = 2$ ), thus showing that the system turns metallic only for a single value of the interaction strength, and not over a range of  $U$  values.

exists only on a single line, rather than a finite range of  $U$  values for any  $V \neq 0$ . It is of course well known that for  $V = 0$ , the usual Hubbard model exhibits a metallic phase for all  $U \leq U_{c2}$ .

In order to consolidate our conclusions from the analytical arguments of section III A 1 and the numerical results from IPT, we have carried out finite temperature CTQMC calculations using the hybridization expansion algorithm. The Fermi-level spectral weight  $\tilde{A}_{1\sigma} = -G_{1\sigma}(\tau = \frac{\beta}{2})/T\pi$  as a function of  $U/W$  for various temperatures ( $\beta = 1/T$ ) are shown in figure 2. We will first focus on the results obtained for the lowest temperature ( $\frac{1}{T} = \beta = 128$ ) that we have reached through our calculations. At low  $U$  value, the Fermi-level spectral weight  $\tilde{A}_{1\sigma}$  is zero up to  $\frac{U}{W} = 0.75$ . Beyond that, it starts increasing with  $U$  and it reaches a maximum value ( $\sim 0.6$ ) around  $\frac{U}{W} = 1.25$ . Then it becomes constant for a range of  $U$  value. As we increase the  $U$ -value further, there is a discrete jump (first order transition) in  $\tilde{A}_{1\sigma}$ , where the DOS at the Fermi-level is zero. This means, for small  $U$ -values we have a band insulator (BI) and for interme-

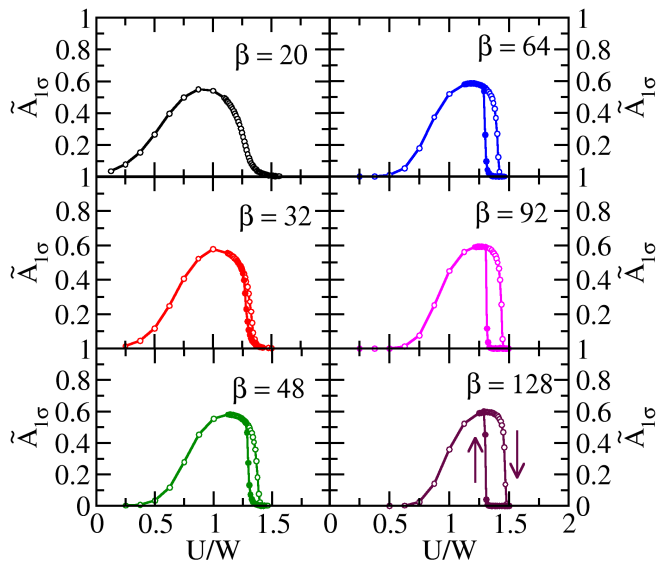


FIG. 2. (color online) Fermi-level spectral weight  $\tilde{A}_{1\sigma}$  as a function of  $U$  for different  $\beta$  values obtained from HY-CTQMC for  $x=1$ . (Down-arrow corresponds to increase in  $U$ , Up-arrow corresponds to decrease in  $U$ , Energy unit  $D = \frac{W}{2} = 1$ )

diate  $U$ -values BI crosses-over ( $U_{co}$ ) to a metal (M) then finally it becomes Mott-insulator (MI) for large  $U$ -values ( $> U_{c1}$ ). At the same temperature ( $\beta = 128$ ), starting with MI state, we reduce the  $U$ -value, system went to a metallic state at  $U_{c2}$  which is smaller than  $U_{c1}$ . The region between critical values ( $U_{c2}, U_{c1}$ ) corresponds to the coexistence region, where M and MI solutions simultaneously exist. As we increase the temperature, beyond  $\beta=32$  the transition from M to MI turns into a crossover. At finite temperature, we observed a metallic region in the ionic Hubbard model rather than a metallic point.

We find the crossover value ( $U_{co}$ ) from BI to M by a linear fit of  $\tilde{A}_{1\sigma}$  to the region where it grows linearly with  $U$ , which has shown in the inset of figure 3. We identified the critical values ( $U_{c2}, U_{c1}$ ) based on low frequency behaviour of imaginary part of self energy (MI state:  $-\text{Im} \Sigma_{1\sigma}(i\omega_n) \propto \frac{1}{\omega_n}$  and M state:  $-\text{Im} \Sigma_{1\sigma}(i\omega_n) \propto \omega_n$ ). We have used the same procedure throughout the chapter to find critical values at each temperature and  $x$ . We have determined the critical values at each temperature, for  $x = 0$  as shown in figure 3. As we increase the temperature, the metallic region which is bounded by two insulators increases (i.e., BI region decreases) and the coexistence region between M and MI decreases and finally disappears at  $\beta=32$ . By extrapolating the critical values in figure 3 to zero temperature, we cannot conclude the existence of metallic phase. However, as we increase the  $U$  value, CTQMC yields the impurity occupancy which is

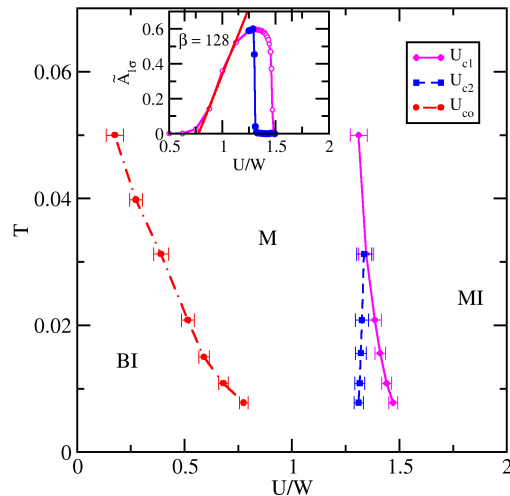


FIG. 3. (color online) Finite temperature phase diagram of Ionic band Insulator ( $x=1.0$ ) obtained from HY-CTQMC (BI: Band Insulator, M: Metal and MI: Mott Insulator), Inset: Linear fit to  $\tilde{A}_{1\sigma}$  in the metallic region at  $\beta=128$ .

always less than 0.5 (i.e.,  $n_{1\sigma} < 0.5$ ). That means there will be a single  $U$  value, where the metallic condition  $\mu - \text{Re}\Sigma_{1\sigma}(0) = V$  satisfies, since  $\text{Re}\Sigma_{1\sigma}(0) < \frac{U}{2}$ . The existence of metallic region at finite temperature in IHM for a broad range of  $U$  values is mainly due to the proximity of existence of metallic point at zero temperature which is confirmed by analytics, IPT, and HY-CTQMC.

## 2. (b) $x=0$ (covalent band insulator)

We have calculated the low energy quasi-particle weight ( $Z$ ) and the gap in the spectral function (charge gap:  $\Delta_c$ ) which are obtained from MO-IPT and plotted in figure 4 as a function of  $U$ . As we increase the  $U$ -value,  $Z$  smoothly decreases, because of correlations. On the other hand, charge gap is also going to zero with  $U$ . However, we did not observe the closing of the gap in the spectral function for any  $U$ -value before the system goes to MI state ( $Z \sim 0$ ). Local electronic correlations in the CBI renormalizes the charge gap, but they cannot close the gap. The critical  $U$  where the system goes from BI to MI is almost at twice the bandwidth because of strong bonding nature of a covalent character.

In figure 5 we have plotted  $\tilde{A}_{1\sigma}$  as a function  $\frac{U}{W}$  for different temperatures. The behavior of  $\tilde{A}_{1\sigma}$  for  $x = 0$  (CBI) is completely different from  $x = 1$  (IHM) case. For example,  $\tilde{A}_{1\sigma}$  is zero up to the large value of  $\frac{U}{W} (=2.0)$  even though both insulators have same bandwidths, i.e., BI phase in CBI persists up to large  $U$  values. The incre-

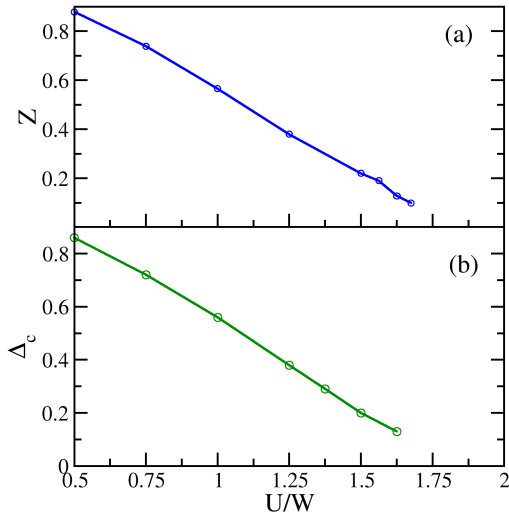


FIG. 4. (color online) (a) Quasi particle weight ( $Z$ ) as a function of  $\frac{U}{W}$  obtained from IPT. (b) Charge gap as a function of  $\frac{U}{W}$  obtained from IPT. (We have used  $\eta = 10^{-2}$  and energy unit is  $D = \frac{W}{2} = 2$ )

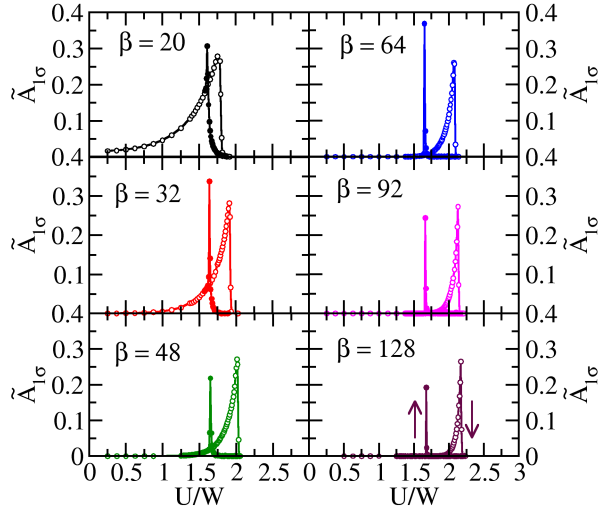


FIG. 5. (color online) Fermi-level spectral weight as a function of  $\frac{U}{W}$  for different  $\beta$  values obtained from HY-CTQMC for  $x=0.0$  (Energy unit  $D = W/2 = 1.0$ )

ment of  $\tilde{A}_{1\sigma}$  with respect to  $U$  increases rather sharp, and it is finite for a narrow range of  $U$  values in compare with IHM. As we increase  $U$ , the system first evolves from BI to M ( $U_{co}$ ) then finally went to MI state at critical  $U_{c1}$ . The transition from M to MI is the first-order type, and it persists even for higher temperatures. For fixed  $\beta$ , we have also calculated the  $\tilde{A}_{1\sigma}$  value by decreasing  $U$  value from MI then system evolves into a BI state at critical  $U_{c2}$ . The region between critical  $U_{c2}$  and  $U_{c1}$

corresponds to the coexistence region, where BI and MI solutions coexist.

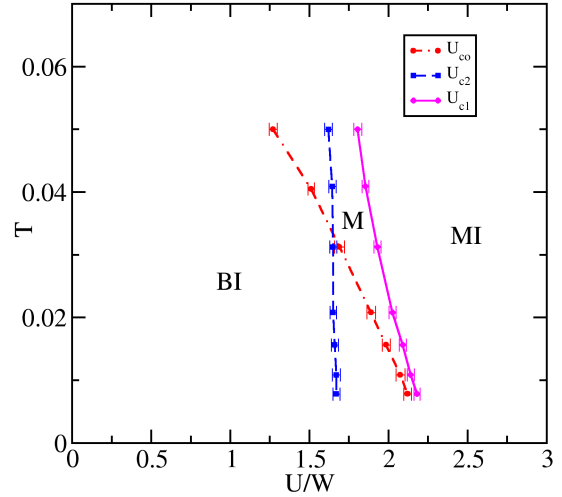


FIG. 6. (color online) Finite temperature phase diagram of Covalent band Insulator ( $x=0.0$ ) on  $T$  Vs  $U$  plane (Energy unit  $D = W/2 = 1.0$ ).

We extracted the critical values at each temperature from the procedure mentioned it earlier and plotted in figure 6. We observed BI phase for a broad range of  $U$  values. At low-temperature metallic region exists for a narrow range of  $U$  values and it broadens as we increase the temperature. The coexistence region ( $U_{c2}$ ,  $U_{c1}$ ) between BI, M, and MI decreases as we increase temperature. The critical values obtained from HY-CTQMC at low temperature confirms that there is no metallic point in CBI at zero temperature, and it is consistent with the analytical arguments and IPT results.

### 3. (c) $x=0.5$ (Equal ratio of ionicity and covalency)

The non-interacting spectral function  $A(\omega) = \rho_{1\sigma}(\omega) + \rho_{2\sigma}(\omega)$  plotted in figure 7 for  $x = 0.5$  has finite DOS at Fermi level and the value is 0.7797, which is good agreement with the analytical expression of  $\sqrt{2}\rho(-V)$  i.e., non-interacting ground state is a metal.

Fermi-level spectral weight  $\tilde{A}_{1\sigma}$  as a function of  $U$  for different temperatures plotted in figure 8. At low temperature ( $\beta=128$ ) as we increase  $U$ , there is a minimum in  $\tilde{A}_{1\sigma}$  before the system went to a MI state and the highest value of 0.6 in  $\tilde{A}_{1\sigma}$  reached at  $\frac{U}{W} = 1.1$ . The extrapolation of  $\tilde{A}_{1\sigma}$  to  $U = 0$  axis confirms there is a finite weight at Fermi-level. There are two metallic regions one is at small  $\frac{U}{W} (< 0.5)$  another one is at large  $\frac{U}{W} (= 1.1)$ . An interaction induced band insulator has emerged in between

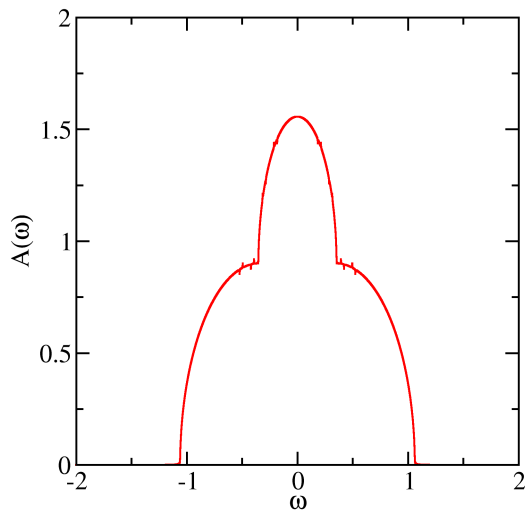


FIG. 7. (color online) Non-interacting spectral function for  $x=0.5$  (We have used  $\eta=10^{-2}$  and energy unit  $= D = \frac{W}{2} = 1$ )

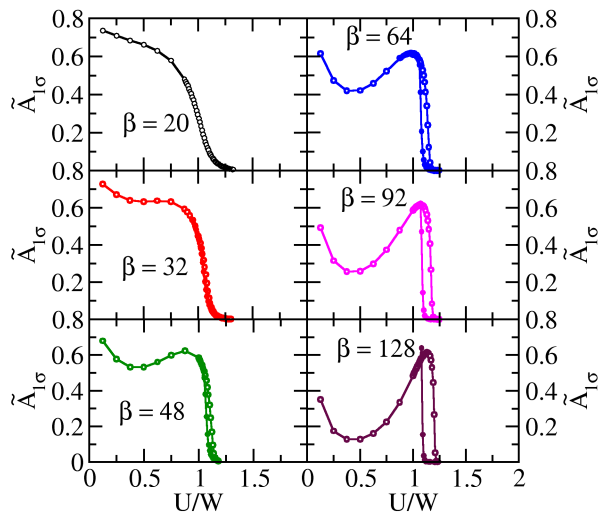


FIG. 8. (color online) Fermi-level spectral weight as a function of  $\frac{U}{W}$  obtained from HY-CTQMC for different  $\beta$  values and  $x=0.5$  (Energy unit  $D = \frac{W}{2} = 1$ ).

these two metallic regions, and MI state is at large  $U$  values. As a function of temperature, the minimum of  $\tilde{A}_{1\sigma}$  which has observed at low-temperature starts filling up.

Next, we need to address whether the metallic behavior observed at low  $U$ -values, is it due to thermal broadening or not? To know this we did low temperature ( $\beta=300$ ) calculations using HY-CTQMC then we plotted  $\tilde{A}_{1\sigma}$  in figure 9(a). The extrapolation of  $\tilde{A}_{1\sigma}$  to  $\frac{U}{W}=0$  axis confirms that there is metal at  $U=0$ , i.e.,

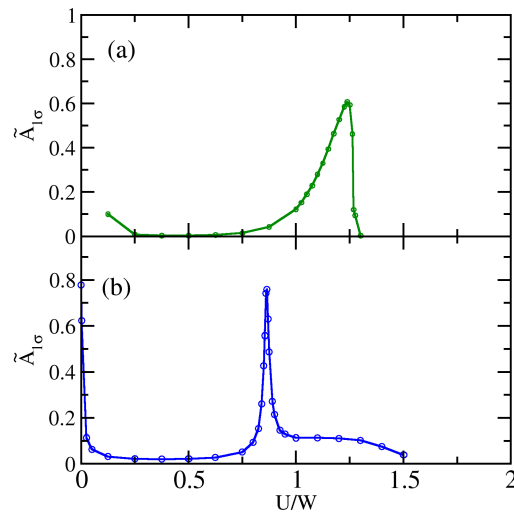


FIG. 9. (color online)(a) Fermi-level spectral weight as a function of  $\frac{U}{W}$  obtained from (a) HY-CTQMC (b) IPT for  $x=0.5$  and  $\beta = 300$ . (We have used  $\eta=10^{-2}$  and energy unit  $D=\frac{W}{2} = 1$ )

the emergence of metal is not due to thermal broadening. Once we turn on  $U$ , then the non-interacting metal turn into a band insulator that means correlations created a band insulator. It is well known that correlations in the metal create MI (charge gap is an order of  $U$ ). The local electronic correlations turn band insulator into a metal seems counter-intuitive, but the creation of band insulator due to electronic correlations seems even more counter-intuitive. Unless low  $U$ -value calculations carried, we do not know the behavior of  $\tilde{A}_{1\sigma}$ . Since HY-CTQMC is a strong coupling method so we have done IPT calculations at  $\beta=300$  and we plotted  $\tilde{A}_{1\sigma}$  as a function of  $\frac{U}{W}$  in the figure 9(b). We can clearly see at  $U=0$ ; there is a metal  $\tilde{A}_{1\sigma} = 0.76$ , which is in close agreement with the exact value derived from the analytical expression. IPT also predicted two metallic regions, a BI region in between them and MI region at large  $U$ . The critical  $U$ -values predicted from IPT are somewhat different from HY-CTQMC, due to the lack of correct strong coupling behavior in the interpolative methods.

In figure 10, we have plotted the critical values as a function of  $\frac{U}{W}$  obtained from HY-CTQMC at different temperatures. According to analytical predictions, metallic behavior which exists at  $U=0$  turns into a BI with an increase of  $U$  and there is a possibility of an existence of second metallic phase at larger  $U$ -value if the condition  $\mu - \text{Re}\Sigma_{1\sigma}(0)=0$  satisfied, before the BI turns into MI. The extrapolation of critical lines to zero temperature axis gives a metallic point at zero  $U$ -value, and it turns into a BI with an increase of  $U$  at criti-



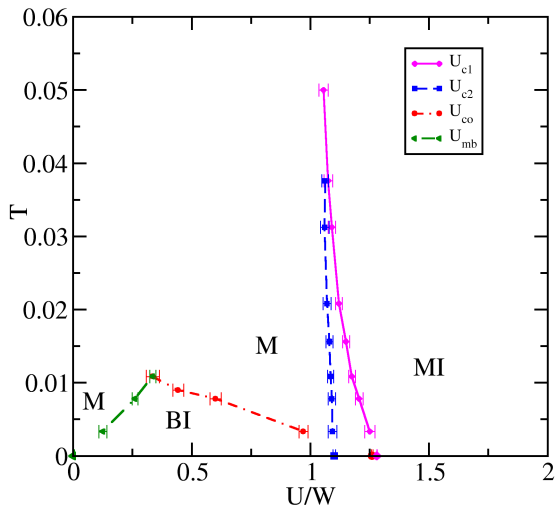


FIG. 10. (color online) Finite temperature phase diagram ( $T$  Vs  $U$ ) for  $x=0.5$  covalency (Energy unit  $D=W/2=1$ ).

cal  $U_{mb}$ . Finally, the BI went to MI state without second metallic phase. The reason for the absence of second metallic phase is because of the metallic condition ( $\mu - \text{Re}\Sigma_{1\sigma}(0)=0$ ) never satisfied, since  $n_{1\sigma} < 0.5$  for any value of  $U$ . At finite temperature, we observed two metallic phases followed by BI and MI insulators up to  $\beta$  of 100 and beyond this, the BI region disappears, and only M and MI regions survives. The metallic behavior observed at finite temperature for large  $U$  values is due to the thermal broadening and the region between critical values ( $U_{c2}, U_{c1}$ ) corresponds to the coexistence of M and MI solutions.

#### 4. (d) $0 > x < 0.5$ and $0.5 > x < 1.0$

Before going to analyze the interacting case results for general  $x$  value, let's focus on the results from the non-interacting case. In figure 11, we have plotted the occupancy of each orbital i.e.,  $n_{1\sigma}$ ,  $n_{2\sigma}$  and the gap in the spectral function as a function of  $x$ , at  $V=0.5$ . When  $x = 1$ , due to staggered ionic potential, the occupancy of orbital 2 is almost filled while the orbital 1 is almost empty and the gap in the spectral function is in order of  $V=0.5$ . As we decrease  $x$  from 1 up to  $x=0.5$ , there is no much change in the orbital occupancies. On the other hand, the gap in the non-interacting spectrum smoothly decreases, and reaches zero at  $x=0.5$ . As we decrease  $x$ , below 0.5, then the occupancy of the orbital 2 decreases while it increases for orbital 1 and the gap in the spectral function increases. For  $x=0$ , the gap reaches a value of 0.5, and the corresponding occupancy of each orbital is 0.5.

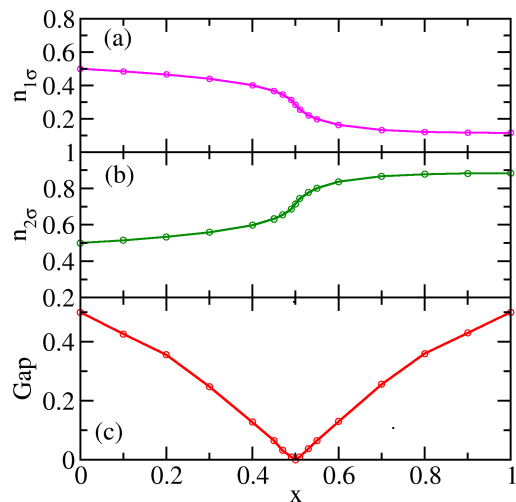


FIG. 11. (color online) Non-interacting occupancy (a) for orbital 1 (b) for orbital 2 and (c) gap in the spectral function as function of  $x$  ( $V = 0.5$  and Energy unit  $=D=\frac{W}{2}=1$ )

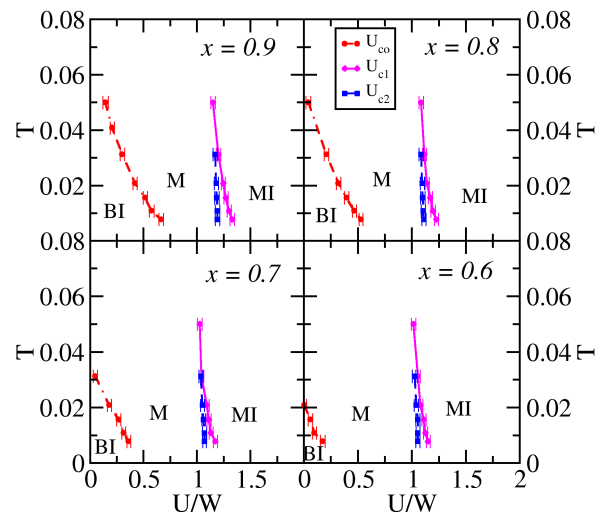


FIG. 12. (color online)  $T$  Vs  $U$  phase diagram for  $0.5 > x < 1.0$  (Energy unit  $= D = \frac{W}{2}=1$ ).

We have calculated the critical values as a function of  $\frac{U}{W}$  for  $0.5 > x < 1.0$  at different temperatures and plotted in figure 12. As we decrease  $x$  from 1, then the metallic region that exists between BI and MI increases (i.e., a small amount of covalency favors metallicity) and the coexistence region between metal and MI decreases. From analytical results we know the condition that needs to be satisfied to get a metallic phase at zero temperature is  $\mu - \text{Re}\Sigma(0) = -\frac{1-2x}{x}$ . It will be satisfied with a single  $U$ -value for  $0.5 > x < 1$  and only when  $n_{1\sigma} < 0.5$ . From finite temperature data, we find  $n_{1\sigma} < 0.5$ , that means

there is a possibility for the existence of metallic point at single  $U$ -value at  $T=0$ . The metallic region observed at finite temperature is not only due to thermal broadening but also from the existence of metallic point at  $T=0$ . As we decrease  $x$  from 1, the critical value  $U_{co}$  decreases. From this, at least we can speculate, the existence of metallic point at  $T=0$  shifts towards low  $U$ -values and it reaches  $U=0$  for some value of  $x$ . Indeed, we determined it for  $x=0.5$ , where the non-interacting ground state itself is a metal.

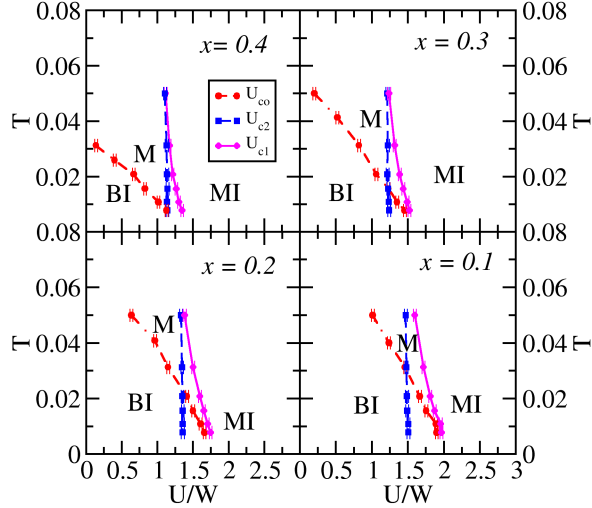


FIG. 13. (color online)  $T$  Vs  $U$  phase diagram for  $0.0 > x < 0.5$  (Energy unit =  $D = \frac{W}{2} = 1$ )

In figure 13, we have plotted the critical values for  $0.0 > x < 0.5$  at different temperatures. As we decrease  $x$  from 0.5, the metallic region sandwiched between BI and MI decreases (i.e., the critical value of crossover from BI to M increases) while the coexistence region between BI and MI increases. At zero temperature, for  $0.0 > x < 0.5$ , the metallic condition  $\mu - \text{Re}\Sigma(0) = -\frac{1-2x}{x}$ , will be satisfied at a single  $U$ -value only when  $n_{1\sigma} > 0.5$ . From finite temperature data, we find  $n_{1\sigma} < 0.5$  which implies that there is no chance of satisfying the metallic condition. The absence of metallic point at zero temperature is also evident from the behavior of critical values in figure 13 at low enough temperature. The metallic region observed at finite temperature for  $0.0 > x < 0.5$  is only due to the thermal broadening.

#### IV. CONCLUSIONS

We have studied the role of local electronic correlations in different kind of band insulators. Our analytical results predict that presence of metallic point in the IHM

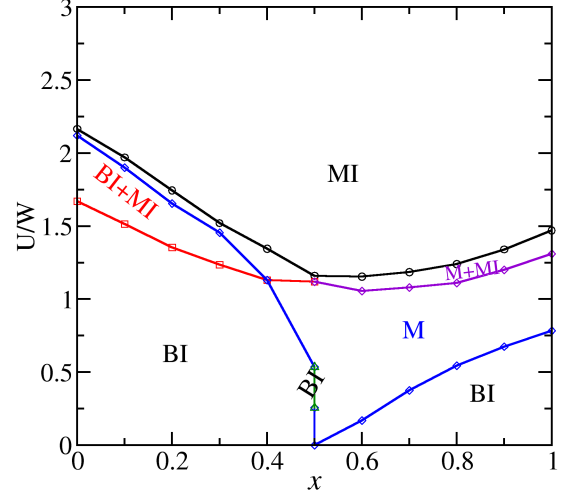


FIG. 14. (color online) Critical  $U$  values Vs  $x$  Phase diagram for  $V = 0.5$  and  $\beta=128$  (Energy unit  $D=W/2=1$ )

model while it is absent in the case of CBI. When ionicity and covalency are in equal ratio, then the non-interacting ground state becomes a metal, but the correlations turn non-interacting metal into a correlated band insulator. We also derived the conditions for the existence of metallic phase for the general case.

The summary of numerical results is plotted in figure 14. Our numerical results confirmed the analytical predictions of the existence of a metallic point in IHM while the absence of it in CBI at zero temperature. For  $x=0.5$ , non-interacting ground state (GS) is a metal, but with correlations GS changes from metal to a Band Insulator. We observed an interaction induced BI when ionicity and covalency are in equal ratio and this phase was counter-intuitive in the sense of our fundamental understanding of correlation effects. The value of  $n_{1\sigma}$  obtained from HY-CTQMC confirms the existence of metallic point at zero temperature for  $0.5 > x < 1.0$  and there is no such point for  $0.0 > x < 0.5$ . The metallic region observed at finite temperature for  $0.5 > x < 1.0$  is much broader than the  $0.0 > x < 0.5$ , since there is no metallic point at zero temperature in the latter case. The electronic correlations favor the metallicity when the covalency is smaller than ionicity, and it has opposite effect when covalency greater than ionicity. Our results will open new directions in the study of electronic correlations in band insulators. The possible experimental systems of relevance for our findings are Titanium-doped perovskite ruthenates  $\text{SrRu}_{1-x}\text{Ti}_x\text{O}_3$  and some of the 3d transition metal oxides with crystal field splitting<sup>32</sup>.

## Acknowledgments

We thank CSIR and DST (India) for research funding. Additional support (MJ) was provided by NSF Materials Theory grant DMR1728457. Our simulations used an open source implementation<sup>33</sup> of the hybridiza-

tion expansion continuous-time quantum Monte Carlo algorithm<sup>34</sup> and the ALPS<sup>31</sup> libraries. The CTQMC simulations were conducted on the computational resources provided by Louisiana Optical Network Initiative (LONI) and HPC@LSU.

- 
- \* [nagamalleswararao.d@gmail.com](mailto:nagamalleswararao.d@gmail.com)  
 † [raja@jncasr.ac.in](mailto:raja@jncasr.ac.in)
- <sup>1</sup> A. M. Turner, A. Vishwanath, and Head, *Topological Insulators* **6**, 293 (2013).
  - <sup>2</sup> X. Chen, Z.-C. Gu, Z.-X. Liu, and X.-G. Wen, *Phys. Rev. B* **87**, 155114 (2013).
  - <sup>3</sup> J. C. Budich, B. Trauzettel, and G. Sangiovanni, *Phys. Rev. B* **87**, 235104 (2013).
  - <sup>4</sup> A. Amaricci, J. C. Budich, M. Capone, B. Trauzettel, and G. Sangiovanni, *Phys. Rev. Lett.* **114**, 185701 (2015).
  - <sup>5</sup> A. P. Kampf, M. Sekania, G. I. Japaridze, and P. Brune, *Journal of Physics: Condensed Matter* **15**, 5895 (2003).
  - <sup>6</sup> S. R. Manmana, V. Meden, R. M. Noack, and K. Schönhammer, *Phys. Rev. B* **70**, 155115 (2004).
  - <sup>7</sup> C. D. Batista and A. A. Aligia, *Phys. Rev. Lett.* **92**, 246405 (2004).
  - <sup>8</sup> A. Garg, H. R. Krishnamurthy, and M. Randeria, *Phys. Rev. Lett.* **97**, 046403 (2006).
  - <sup>9</sup> S. S. Kancharla and E. Dagotto, *Phys. Rev. Lett.* **98**, 016402 (2007).
  - <sup>10</sup> L. Craco, P. Lombardo, R. Hayn, G. I. Japaridze, and E. Müller-Hartmann, *Phys. Rev. B* **78**, 075121 (2008).
  - <sup>11</sup> N. Paris, K. Bouadim, F. Hebert, G. G. Batrouni, and R. T. Scalettar, *Phys. Rev. Lett.* **98**, 046403 (2007).
  - <sup>12</sup> K. Byczuk, M. Sekania, W. Hofstetter, and A. P. Kampf, *Phys. Rev. B* **79**, 121103 (2009).
  - <sup>13</sup> A. J. Kim, M. Y. Choi, and G. S. Jeon, *Phys. Rev. B* **89**, 165117 (2014).
  - <sup>14</sup> A. Hoang, *Journal of Physics: Condensed Matter* **22**, 095602 (2010).
  - <sup>15</sup> M. Sentef, J. Kuneš, P. Werner, and A. P. Kampf, *Phys. Rev. B* **80**, 155116 (2009).
  - <sup>16</sup> A. Euverte, S. Chiesa, R. T. Scalettar, and G. G. Batrouni, *Phys. Rev. B* **87**, 125141 (2013).
  - <sup>17</sup> P. Werner and A. J. Millis, *Phys. Rev. Lett.* **99**, 126405 (2007).
  - <sup>18</sup> G. Moeller, V. Dobrosavljević, and A. E. Ruckenstein, *Phys. Rev. B* **59**, 6846 (1999).
  - <sup>19</sup> A. Fuhrmann, D. Heilmann, and H. Monien, *Phys. Rev. B* **73**, 245118 (2006).
  - <sup>20</sup> S. S. Kancharla and S. Okamoto, *Phys. Rev. B* **75**, 193103 (2007).
  - <sup>21</sup> M. Fabrizio, *Phys. Rev. B* **76**, 165110 (2007).
  - <sup>22</sup> H. Hafermann, M. I. Katsnelson, and A. I. Lichtenstein, *EPL (Europhysics Letters)* **85**, 37006 (2009).
  - <sup>23</sup> J. Kuneš and V. I. Anisimov, *Phys. Rev. B* **78**, 033109 (2008).
  - <sup>24</sup> Z. Schlesinger, Z. Fisk, H.-T. Zhang, M. B. Maple, J. DiTusa, and G. Aeppli, *Phys. Rev. Lett.* **71**, 1748 (1993).
  - <sup>25</sup> C. Petrovic, Y. Lee, T. Vogt, N. D. Lazarov, S. L. Bud'ko, and P. C. Canfield, *Phys. Rev. B* **72**, 045103 (2005).
  - <sup>26</sup> C. Kittel, "Introduction to solid state physics, 8th edition," (Wiley, 2004) Chap. CRYSTAL BINDING AND ELASTIC CONSTANTS, pp. 47–85.
  - <sup>27</sup> Ashcroft/Mermin, "Solid state physics," (THOMSON BROOKS/COLE, 2007) Chap. Classification of Solids, pp. 373–393.
  - <sup>28</sup> J. E. Han, M. Jarrell, and D. L. Cox, *Phys. Rev. B* **58**, R4199 (1998).
  - <sup>29</sup> N. Dasari, W. R. Mondal, P. Zhang, J. Moreno, M. Jarrell, and N. S. Vidhyadhiraja, *The European Physical Journal B* **89**, 202 (2016).
  - <sup>30</sup> P. Werner, A. Comanac, L. de' Medici, M. Troyer, and A. J. Millis, *Phys. Rev. Lett.* **97**, 076405 (2006).
  - <sup>31</sup> B. Bauer, L. D. Carr, H. G. Evertz, A. Feiguin, J. Freire, S. Fuchs, L. Gamper, J. Gukelberger, E. Gull, S. Guertler, A. Hehn, R. Igarashi, S. V. Isakov, D. Koop, P. N. Ma, P. Mates, H. Matsuo, O. Parcollet, G. Pawowski, J. D. Picon, L. Pollet, E. Santos, V. W. Scarola, U. Schollwck, C. Silva, B. Surer, S. Todo, S. Trebst, M. Troyer, M. L. Wall, P. Werner, and S. Wessel, *Journal of Statistical Mechanics: Theory and Experiment* **2011**, P05001 (2011).
  - <sup>32</sup> K. Maiti, R. S. Singh, and V. R. R. Medicherla, *Phys. Rev. B* **76**, 165128 (2007).
  - <sup>33</sup> H. H. Hafermann, P. Werner, and E. Gull, *Computer Physics Communications*, **184**, 1280 (2013).
  - <sup>34</sup> P. Werner, A. Comanac, L. de' Medici, M. Troyer, and A. J. Millis, *Phys. Rev. Lett.* **97**, 076405 (2006).